PROCEEDINGS OF SPIE

SPIEDigitalLibrary.org/conference-proceedings-of-spie

Single-particle imaging for biosensor applications

Mustafa Yorulmaz, Cagatay Isil, Elif Seymour, Celalettin Yurdakul, Berkan Solmaz, et al.

SPIE.

Single-Particle Imaging for Biosensor Applications

Mustafa Yorulmaz[a], Cagatay Isil[a], Elif Seymour[a], Celalettin Yurdakul[b], Berkan Solmaz[a], Aykut Koc[a], M. Selim Ünlü[b, c]
[a]ASELSAN Research Center, Ankara 06370, Turkey; [b]Department of Electrical and Computer Engineering, Boston University, Boston, Massachusetts 02215, USA; [c]Department of Biomedical Engineering, Boston University, Boston, Massachusetts 02215, USA

ABSTRACT

Current state-of-the-art technology for in-vitro diagnostics employ laboratory tests such as ELISA that consists of a multi-step test procedure and give results in analog format. Results of these tests are interpreted by the color change in a set of diluted samples in a multi-well plate. However, detection of the minute changes in the color poses challenges and can lead to false interpretations. Instead, a technique that allows individual counting of specific binding events would be useful to overcome such challenges. Digital imaging has been applied recently for diagnostics applications. SPR is one of the techniques allowing quantitative measurements. However, the limit of detection in this technique is on the order of nM. The current required detection limit, which is already achieved with the analog techniques, is around pM. Optical techniques that are simple to implement and can offer better sensitivities have great potential to be used in medical diagnostics. Interference Microscopy is one of the tools that have been investigated over years in optics field. More of the studies have been performed in confocal geometry and each individual nanoparticle was observed separately. Here, we achieve wide-field imaging of individual nanoparticles in a large field-of-view (~166 μm x 250 μm) on a micro-array based sensor chip in fraction of a second. We tested the sensitivity of our technique on dielectric nanoparticles because they exhibit optical properties similar to viruses and cells. We can detect non-resonant dielectric polystyrene nanoparticles of 100 nm. Moreover, we perform post-processing applications to further enhance visibility.

Keywords: Interference Microscopy, wide-field imaging, digital counting, single-particle, polystyrene, deconvolution, post-processing

1. INTRODUCTION

Infectious diseases have become a major problem worldwide with increasing importance. Therefore, the need for systems which can timely detect infectious agents is increasing especially for early diagnosis and treatment.[1, 2] Protein biomarkers are successful identifiers of diagnosis and prognosis in a variety of diseases from cancer to allergy.[3, 4] Disease state and progression can be determined by the measurement of the related biomarker. For example, the survival rate for colorectal, breast and prostate cancers have increased due to improvement in early detection and technological advances resulting in better treatment.[5]

Enzyme-Linked ImmunoSorbent Assay (ELISA) and Polymerase Chain Reaction (PCR) are currently gold standards in the diagnostics industry. ELISA consists of immobilization of an unknown amount of antigen into a well-plate, adding the patient sample that contains the antibody which is produced in response to an infection, coming in with a specific antibody labeled with an enzyme, and then adding a substrate that reacts with the enzyme to produce a color change.[6] PCR provides very sensitive identification of many pathogens by amplifying the corresponding nuclear acid target.[7] Even though these ELISA and PCR provide accurate and sensitive measurements, they require significant sample preparation, a trained person in order to apply the technique. Moreover, the tests are hard to miniature and costly.

The concentration of the proteins for typical clinical measurements are on the order of $\sim 10^{-12}$ M.[8] Among the technological advances for new generation diagnostics, biosensors become promising for clinical use due to their sensitivities and ease of use. Biosensors are shown in literature to find applications in diagnostics from allergy to cancer. For diagnostics of cancer, neurological disorders, and the early stages of infection, more sensitive protein diagnostics tools are required. Because for this aforementioned monitoring, measurement of the proteins with concentration in the range of $10^{-16} – 10^{-12}$ M in serum is required.[9-11]

Emerging Imaging and Sensing Technologies for Security and Defence II, edited by Keith L. Lewis, Richard C. Hollins, Gerald S. Buller, Robert A. Lamb, Proc. of SPIE Vol. 10438, 104380I
 · doi: 10.1117/12.2279005

Development of highly sensitive, quantitative, and multiplexed biomarker detection systems at the point of care is a crucial focus for the technological development of next generation diagnostics.[12] An idealized POC diagnostic test should be similar to a pregnancy or glucose monitoring test, i.e., very simple, easy to use, and easy to interpret.[13]

There have been attempts for digital detection of biomolecules for clinical applications. Developing techniques in order to image nanoparticles for early detection of diseases, such as viral infections and cancer, as well as the use of nanoparticles for the treatment of certain types of cancers has recently gained considerable attention. It has been shown that bio-agents of concentration of ~fM can be measured optically.[14]

We aim to develop an in-vitro point-of-care biosensor that can be used for diagnostic purposes. For this purpose, an imaging technique that is sensitive, easy-to-implement, low-cost, and easy-to-miniaturize is essential. Such a technique will be useful to develop biosensors which will transform into portable medical imaging and detection devices, allowing for disease diagnostics in remote locations and subsequent planning for clinical therapy.

Optical interferometric techniques have proven utility in sensitive imaging of individual nanoparticles in wide-field. We further study this technique and implement various optical schemes to improve the sensitivity of this biosensor, targeting to detect smaller biomolecules that would normally go undetected with the current system. Applying post-processing tools to the acquired images allows increasing the optically achieved resolution and contrast.

2. WIDE-FIELD INTERFERENCE MICROSCOPY FOR SINGLE PARTICLE IMAGING AND COUNTING

Single-particle imaging and spectroscopy is important for applications in chemistry, biology and soft matter systems.[15, 16] Different optical schemes employing interference of light has been applied in literature for detection of individual nanoparticles.[17, 18] Label-free optical sensing down to single-molecule level and spectroscopy of gold nanoparticles down to 10 nm was enabled by Interferometric Scattering Microscopy.[19, 20] Enhanced signal levels in detection of low-index, non-resonant dielectric nanoparticles were demonstrated by pupil function engineering in common-path Interferometric Microscopy.[21] In Photothermal Microscopy, small modulated changes in the detected probe light is generated by interference of the reference field and the scattered field, which is modulated at a certain frequency. Lock-in detection is employed to isolate the small modulated component, providing the sensitivity of absorption measurement down to a single chromophore.[22] All of these measurements allow sensitive detection. However, the image of each nanoparticle can be recorded by raster scanning of the sample across the tightly focused excitation light. Therefore, recording the images of nanoparticle on a large area is slow. Moreover, because the excitation has to be performed using supercontinumm or single mode laser light sources and piezo stages with high positioning accuracy has to be used for raster scanning, confocal interference microscopy is costly.

In our wide-field interferometric detection of nanoparticles, we image the nanoparticles that are deposited on the SiO_2 surface or captured by the biomolecules spotted on the SiO_2 surface.

The sample is excited by an incident beam, E_{inc}. Part of the excitation light is scattered off by the nanoparticles (E_s) with a magnitude proportional to the scattering cross-section (σ_{sca}) of the nanoparticle. In addition, part of it is reflected off from the air/substrate interface. The measured signal is the magnitude square of the sum of the reference (in this case reflected) and scattering fields within the numerical aperture (NA) of the system. The signal is affected by the phase difference between the reference field and the scattering field. (Eqn. 1).

The signal that is registered on the photodetector is then written as in the following:

$$I \propto \left|E_s + E_r\right|^2 \propto \left|E_r\right|^2 + \left|E_s\right|^2 - 2\left|E_r\right|\left|E_s\right|\cos\left(\theta_{rs}\right) \tag{1}$$

The excitation and collection geometry is sketched in Fig. 1 for better visualization.

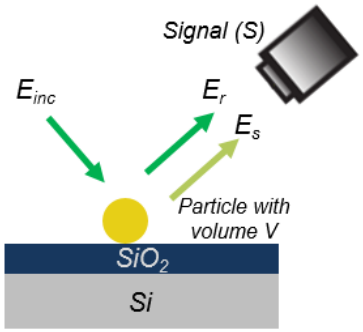

Figure 1. The schematic representation of the sample excitation, signal generation and collection conditions.

The interferometric detection of scattering signal generated by the nanoparticle upon its excitation with the light source is different than in the case of detecting the direct scattered light, such as the scattering signal in the dark field scattering microscopy. The signal measured using the solely scattering-based detection techniques scales as follows:

$$I \propto |E_s|^2 \tag{2}$$

where $|E_s|^2$ is the direct scattering signal and E_s is scattering field. As E_s scales with r^6, the direct scattering signal scales with r^6 and drops notably for nanoparticles with small sizes. For example, it becomes very challenging to image gold nanoparticles with sizes below 40 nm using direct scattering signal.[23]

On the other hand, the intensity measured using an interferometric system is as follows:

$$I \propto 2|E_r||E_s|\cos(\theta_{rs}) \tag{3}$$

where E_r is the reference field and the interference signal that is the cross-term scales with r^3. Therefore, interferometric methods allow imaging nanoparticles with smaller sizes. Moreover, provided that the θ_{rs} (phase between the reflected and scattered field) is controlled, the measured signal can further be improved.

We put efforts in creating practical, robust, and cost-effective solutions for non-laboratory environments. Moreover, imaging and counting of nanoparticles deposited on a large area is required for clinical applications. In order to perform sensitive digital imaging of nanoparticles on an individual basis, we successfully implemented and applied the Wide-field Interferometric Microscopy technique and detect metallic and synthetic non-resonant nanoparticles. In spite of the strong imaging capability of the technique, it does not require advanced optics parts. Moreover, it can be developed using single color LED instead of expensive lasers. It requires the use of a silicon-silicon dioxide substrate as a common-path interferometer.

While our technique works in a way similar to confocal interference microscopy, we employ a special substrate in order to perform the interference microscopy in the wide-field. We use a Si/SiO_2 substrate with a certain thickness of SiO_2 (~100 nm), which enables adjustment of the phase (θ_{rs}) between the scattered field and the reference field to maximize the interference signal. The atomically flat surface of the Si allows the same excitation condition for all nanoparticles over a large area.

We perform Wide-Field Interferometric Microscopy in the reflection geometry for single-particle scattering imaging illustrated in Fig. 2. We use an LED performing at 530 nm (Thorlabs M530L3) as illumination source. After the excitation light is fed into the integrating sphere (Thorlabs IS200-4) and the light passes the bandpass filter (Thorlabs FL514.5-3), we direct the beam through a 30 mm lens (Thorlabs AC254-030-A-ML). We create a near collimated excitation light traveling toward the beam splitter which directs the beam toward the microscope objective (Nikon TU Plan Fluor Epi P 50x Obj 0.8NA). Two iris diaphragms (Thorlabs SM1D12D) are used in proper places for controlling the NA of the excitation beam and the field-of-view. A 60 mm lens (Thorlabs AC254-060-A-ML) before the 50/50 beamsplitter (Thorlabs CCM1-BS013) allows the focusing of the excitation light at the back focal plane of the microscope objective. Köhler type wide-field illumination is achieved. We perform Köhler illumination to uniformly

excite the nanoparticles and minimize the image artifcats owing to LED structure. For our objective, we use a 200 mm lens (Thorlabs AC254-030-A-ML) as the tube lens in the microscope. The signal from the nanoparticles is then recorded on the CCD (Point Grey GS3-U3-120S6M-C) camera.

The schematic diagram of our Wide-field Interferometric Microscopy is shown in Fig. 2.

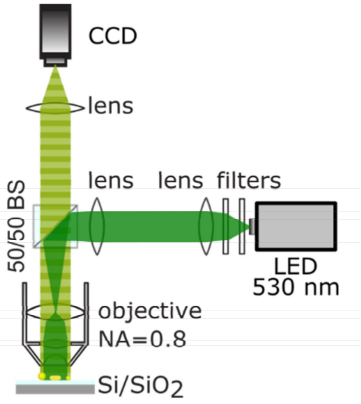

Figure 2. Schematic diagram of the Wide-field Interferometric Microscopy in reflection mode.

After setting up the wide-field imaging system utilizing interference microscopy, we used 1951 USAF resolution test target (Thorlabs R1DS1P) in order to determine the pixel size of our system. We measured the 7th group on this test target (Fig. 3). On the seventh group, the bars and spacings of 1st, 2nd and 3rd units are 3.91 µm, 3.47 µm and 3.11 µm, accordingly. Using this measurement, we determined the relative size of each pixel in our recorded images to be about 59 nm. This value is very close to the expected value of 62 nm, calculated according to the pixel size of the CCD of 3.1 µm and magnification of the objective of 50×.

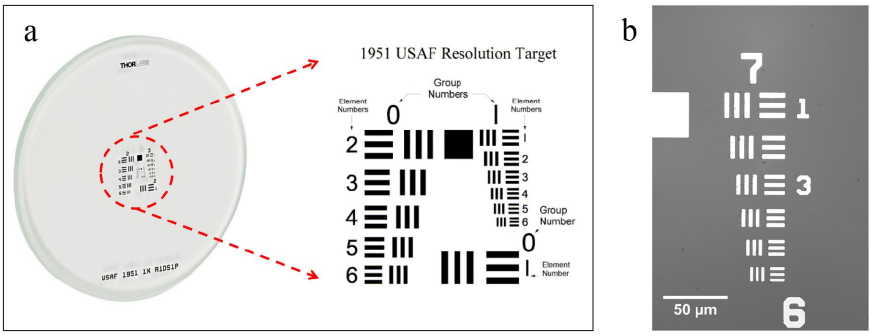

Figure 3. a) 1951 USAF resolution test target with magnified image of different groups including bars of different sizes in each unit. b) Image of the 7th group on the test target recording using the microscope system explained in this manuscript. 1st and 3rd units are represented by numbers besides them.

Using this technique, it is possible to image individual gold nanoparticles and also dielectric nanoparticles with smaller scattering cross-sections than those of metal nanoparticles. It is important to test the capability of the system on the detection of dielectric nanoparticles especially because they exhibit dielectric properties similar to biomolecules and cells and we aim to employ our imaging technique in biosensor applications.

3. IMAGING OF DIELECTRIC NANOPARTICLES

A wide-field image of polystyrene nanoparticles was obtained using Wide-field Interferometric Microscopy. Samples of polystyrene nanoparticles in diameters of 150 nm and 100 nm were prepared by spin-coating diluted suspension of nanoparticles on Si/SiO_2 substrate. Homogeneous distribution of nanoparticles over the sample was ensured. No embedding medium was used throughout the optical experiments.

We first imaged 150 nm polystyrene nanoparticles in order to verify the operation of our Wide-field Interference Microscope. While the lengths of recorded image are 166 µm ± 250 µm, we show a cropped area (30 µm ± 30 µm) in Fig. 4a for better visualization. Each spot in Fig. 4a correspond to individual 150 nm diameter gold nanoparticles except for a few aggregates and smaller nanoparticles. For example, the nanoparticle shown in red square is probably an aggregate. Likewise, the nanoparticle in green circle is probably a particle with a diameter smaller than 150 nm. This can be understood by the fact that the interference signal scales with the volume of the nanoparticle. The majority of the nanoparticles in this image show signals similar to each other and we can say that they belong to the batch of similar-sized nanoparticles.

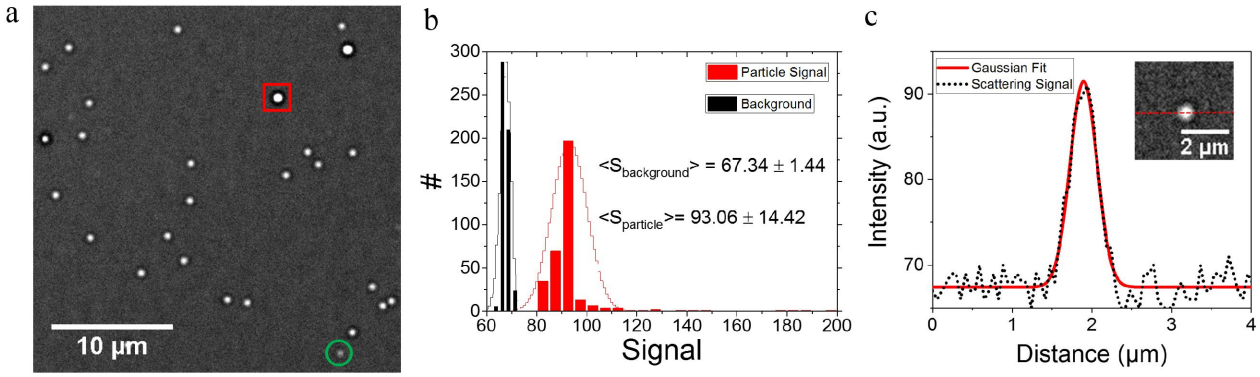

Figure 4. a) The scattering signal of 150 nm polystyrene nanoparticles. b) Histogram of individual nanoparticles' signal and background signal. c) Lines profile over an individual nanoparticle with a Gaussian fit which yielded a spot size of ~397 nm.

We can understand the above explanations further from the distribution of signals of nanoparticles shown in Fig. 4b. The red bars correspond to the signals of 324 particles imaged in larger area and plotted here for better statistics. We observe a singular narrow distribution of signal and the average is 93.06 with a distribution of 15% around the mean. A few particles with higher signals than the envelope of the distribution are observed. In addition, rest of the signals we measure are largely separated from the background signal (black bars in Fig. 4b) and we observe 150 nm diameter polystyrene nanoparticles with a good contrast, which is important for digital counting.

We check the size and shape of the scattering signal spots measured using our imaging method. This analysis helps us to determine whether the alignment of the system was adjusted well. We show the line profile of the signal over a nanoparticle along red-dash line shown in the inset of Fig. 4c. The profile exhibits a nice Gaussian profile. The wavelength of our excitation light is 530 nm and we use 0.8 N.A. objective. The diffraction limited spot ($\sigma = 1.22\frac{\lambda}{2NA}$) should be around 404 nm. We find the FWHM of the measured spot through Gaussian fit as 397 nm experimentally and this result fits well with the expectation.

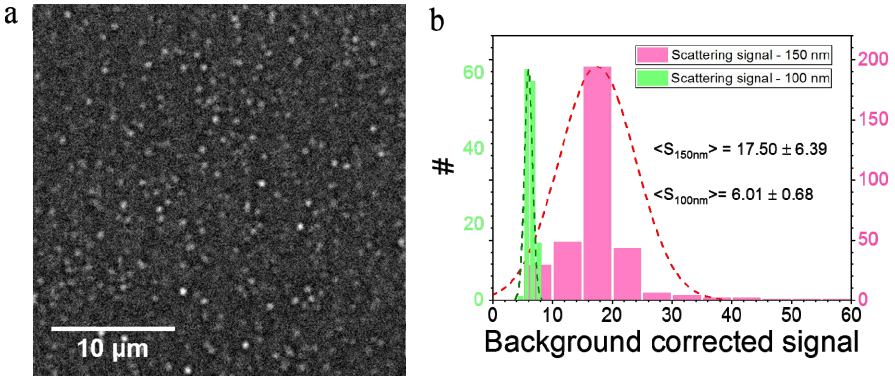

Figure 5. a) The scattering signal of 100 nm polystyrene beads. b) Distribution of signals measured from 150 nm and 100 nm diameter polystyrene nanoparticles.

In order to test the sensitivity of our system for sizes similar to viruses, we imaged smaller diameter of polystyrene nanoparticles than 150 nm. We show the signals of 100 nm diameter polystyrene nanoparticles in Fig. 5a. It appears that the sample is denser than the sample of 150 nm. Even though the contrast is low for this sample it is possible to separate the nanoparticles from the background signal. In order to see the difference of signals between samples of 150 nm and 100 nm diameter polystyrene beads, we plotted the distribution of background corrected signals for these two samples. For this investigation, we did not take into account the signals which we assume are aggregates based on their signals and normal envelopes around the distributions. The average signals for 150 nm and 100 nm diameters samples are 17.5±6.39 and 6.01±0.68, respectively. The average interference scattering signal of 150 nm diameter particles is 2.91 times larger than that of 100 nm. This results matches well with the theory that interference signal directly scales with the volume of nanoparticles ($\frac{150^3}{100^3} = 3.38$). The small discrepancy between the measured and expected dependencies could be due to that fact that it is harder to analyze signals of nanoparticles with dimmer spots observed in Fig. 5a. Therefore, a post-processing technique to increase the contrast will be very helpful. This achievement will improve the results of optical detection and digital counting.

4. CONTRAST AND RESOLUTION ENHANCEMENT USING GENERIC IMAGE PROCESSING ALGORITHMS

In this study, in order to enhance resolution and contrast of images of 100 nm and 150 nm sized polystyrene particles, generic denoising and deblurring algorithms are used.

First, as a denoising algorithm, a moving average filter is used. Moving average filter is a low pass filter, averaging with a finite support along the data points.[24] This filter is formulated as in Eqn. 4,

$$y[n] = \frac{1}{m}\sum_{k=0}^{m-1} x[n-k] \tag{4}$$

where m is the filter length.

After denoising, iterative blind deconvolution algorithm is used in order to have enhanced resolution of images. Blind deconvolution is performed without explicit knowledge of a point spread function (PSF) in imaging. This can be achieved by making appropriate estimations on distribution of point spread function. There are iterative and non-iterative algorithms for blind deconvolution in the literature.[25-26] In this study, an iterative blind deconvolution algorithm which takes advantage of maximum likelihood method is used.[28]

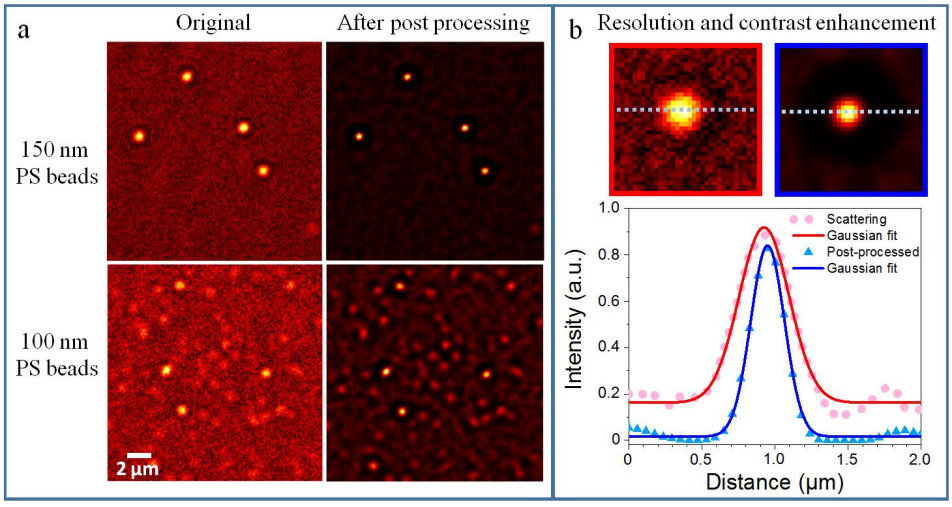

Figure 6. a) The original and post-processed images of 100 nm and 150 nm diameter polystyrene beads. Color scales for the images are kept the same. b) The magnified image of an individual nanoparticle before and after post-processing. The intensity as a function of the distance along the dotted lines on the images is plotted for original and post-processed single particle image.

For sake of convenience, using Matlab implementation of a moving average filter, 1-D filter is applied along both horizontal and vertical directions on images. The length of filter is chosen as 3. Using Matlab implementation of iterative blind deconvolution, the implementation needs initially estimated PSF and the number of iterations. As an initial PSF, normalized 2-D gaussian with standard deviation of 5 and 80×80 support is used. We select the number of iterations as 10. The results are depicted in Fig. 6.

The contrast and the resolution of the image is enhanced after post-processing the data. We show the original images and the images after post-processing for 150 nm and 100 nm diameter particles (Fig. 6a). For both images, it is observed that the sizes of the spots for each spot are decreased while the contrast is increased. We analyze the result further on an individual nanoparticle in Fig. 6b. We plot the line profiles along the dotted lines as shown in the upper part of Fig 6b. The colors of squares are representing the color of the line profiles. We see that the FWHM is decreased from 402 nm to 271 nm. Moreover, the background is largely suppressed and the contrast is largely increased.

5. CONCLUSION

Using our developed Wide-field Interferometric Microscopy, we were able to detect non-resonant, low-index dielectric nanoparticles and record their diffraction limited optical images. The diameters of the polystyrene nanoparticles were 150 nm and 100 nm. They were similar to biological nanoparticles in size and dielectric properties. The post-processing algorithms we applied here further increased the detection sensitivity and resolution. These results provide a sensitive, easy-to-implement, low-cost, and easy-to-miniaturize system which will enable highly sensitive, quantitative, and multiplexed measurements. Therefore, we anticipate that our results will promote further studies of new generation diagnostics.

REFERENCES

[1] Okware, S. I., Omaswa, F. G., Zaramba, S., Opio, A., Lutwama, J. J., Kamugisha, J., Rwaguma, E. B., Kagwa, P. and Lamunu, M., "An outbreak of Ebola in Uganda," Tropical Medicine & International Health, 7, 1068–1075 (2002)

[2] Formenty, P., Leroy, E. M., Epelboin, A., Libama, F., Lenzi, M., Sudeck, H., Yaba, P., Allarangar, Y., Boumandouki, P., Nkounkou, V. B., Drosten, C., Grolla, A., Feldmann, H. and Roth, C., "Detection of Ebola Virus in Oral Fluid Specimens during Outbreaks of Ebola Virus Hemorrhagic Fever in the Republic of Congo," Clinical Infectious Diseases, 42(11), 1521-1526 (2006)

[3] Huang, X. and El-Sayed, M. A., "Gold nanoparticles: Optical properties and implementations in cancer diagnosis and photothermal therapy," Journal of Advanced Research, 1(1), 13-28 (2010)

[4] Yezhelyev, M.V., Gao, X., Xing, Y., Al-Hajj, A., Nie, S. and O'Regan, R. M., "Emerging use of nanoparticles in diagnosis and treatment of breast cancer," Lancet Oncol., 7(8), 657-667 (2006)

[5] Bohunicky, B. and Mousa, S. A., "Biosensors: the new wave in cancer diagnosis," Nanotechnol. Sci. Appl. 4, 1–10 (2011)

[6] Rissin, D. M., Kan, C. W., Campbell, T. G., Howes, S. C., Fournier, D. R., Song, L., Piech, T., Patel, P. P., Chang, L., Rivnak, A. J., Ferrell, E. P., Randall, J. D., Provuncher, G. K., Walt, D. R. and Duffy, D. C., "Single-molecule enzyme-linked immunosorbent assay detects serum proteins at subfemtomolar concentrations," Nature Biotechnology 28, 595–599 (2010)

[7] Lehmann, L. E., Hunfeld, K. P., Emrich, T., Haberhausen, G., Wissing, H., Hoeft, A. and Stüber, F., "A multiplex real-time PCR assay for rapid detection and differentiation of 25 bacterial and fungal pathogens from whole blood samples," Med Microbiol Immunol. 197(3), 313-324 (2008)

[8] Giljohan, D. A. and Mirkin, C. A., "Drivers of biodiagnostic development," Nature 462, 461-464 (2009)

[9] Srinivas, P. R., Kramer, B. S. and Srivastava, S., "Trends in biomarker research for cancer detection," Lancet Oncol. 2(11), 698-704 (2001)

[10] Galasko, D., "Biomarkers for Alzheimer's disease--clinical needs and application," J. Alzheimers Dis. 8(4), 339-346 (2005)

[11] de Jong D., Kremer, B. P., Olde Rikkert M. G. and Verbeek, M. M., "Current state and future directions of neurochemical biomarkers for Alzheimer's disease," Clin. Chem. Lab. Med. 45(11), 1421-1434 (2007)

[12] Vashist, S. K., Luppa, P. B., Yeo, L. Y., Ozcan, A. and Luong, J. H., "Emerging Technologies for Next-Generation Point-of-Care Testing," Trends Biotechnol. 33(11), 692-705 (2015)

[13] Mansuy, J. M., "Mobile laboratories for Ebola and other pathogens," Lancet. Infect. Dis. 15(10), 1135 (2015)
[14] Scherr, S. M., Daaboul, G. G., Trueb, J., Sevenler, D., Fawcett, H., Goldberg, B., Connor, J.H. and Ünlü, M. S., "Real-Time Capture and Visualization of Individual Viruses in Complex Media," ACS Nano 10(2), 2827-2833 (2016).
[15] Zijlstra, P. and Orrit, M., "Single metal nanoparticles: optical detection, spectroscopy and applications," Rep. Prog. Phys. 74(10), 106401 (2011)
[16] Olson, J., Dominguez-Medina, S., Hoggard, A., Wang, L. –W., Chang, W. –S. and Link, S. "Optical characterization of single plasmonic nanoparticles," Chem. Soc. Rev. 44, 40-57 (2015)
[17] Sevenler, D. D., Avci, O. and Ünlü, M. S., "Quantitative interferometric reflectance imaging for the detection and measurement of biological nanoparticles," Biomedical Optics Express 8(6), 2976-2989 (2017)
[18] Avci, O., Adato, R., Yalcin, A. and Ünlü, M. S., "Physical Modeling of Interference Enhanced Imaging and Characterization of Single Nanoparticles," Optics Express 24(6), 6094-6114 (2016)
[19] Lindfors, K., Kalkbrenner, T., Stoller, P. and Sandoghdar, V. Detection and spectroscopy of gold nanoparticles using supercontinuum white light confocal microscopy, Physical Review Letters 93, 037401 (2004).
[20] Arroyo, J. O., Cole, D. and Kukura, P., "Interferometric scattering microscopy and its combination with single-molecule fluorescence imaging," Nature Protocols 11, 617–633 (2016)
[21] Avci, O., Campana, M. I., Yurdakul, C., Ünlü, M. S., "Pupil function engineering for enhanced nanoparticles visibility in wide-field interferometric microscopy," Optica 4(2), 247-254 (2017)
[22] Gaiduk, A., Yorulmaz, M., Ruijgrok, P. V. and Orrit, M., "Room-temperature detection of a single molecule's absorption by photothermal contrast," Science 330(6002), 353-356 (2010)
[23] van Dijk, M. A., Tchebotareva, A. L., Orrit, M., Lippitz, M., Berciaud, S., Lasne, D., Cognet, L. and Lounis, B., "Absorption and scattering microscopy of single metal nanoparticles," Physical Chemistry Chemical Physics 8, 3486 (2006)
[24] Oppenheim, A. V. and Schafer RW., [Discrete-time Signal Processing], Prentice Hall (1999).
[25] Biggs, D. S. C. and Andrews, M., "Acceleration of iterative image restoration algorithms," Applied Optics 36(8), 1766-1775 (1997)
[26] Hanisch, J. R., White, R. L. and Gilliland, R. L., "Deconvolution of Hubble Telescope Images and Spectra," Deconvolution of Images and Spectra, 310-360 (1996)
[27] Holmes, T. J., et al., "Light microscopic images reconstructed by maximum likelihood deconvolution," Handbook of biological confocal microscopy. Springer US, 389-402 (1995)
[28] Lam, E. Y. and Goodman, J. W., "Iterative statistical approach to blind image deconvolution," J. Opt. Soc. Am. A17, 1177-1184 (2000)